Analyst

Reduced acoustic resonator dimensions improve focusing efficiency of bacteria and submicron particles

Journal:	*Analyst*
Manuscript ID	AN-ART-10-2021-001891.R1
Article Type:	Paper
Date Submitted by the Author:	02-Nov-2021
Complete List of Authors:	Ugawa, Masashi; The University of Tokyo, RCAST Lee, Hoyoen; Hanyang University Baasch, Thierry; Lund University, Department of Biomedical engineering Lee, Min-Ho; Chung-Ang University, School of Integrated Engineering Kim, Soyun; Korea University; PCL inc Jeong, Ok Chan; Inje University Choi, Yong-Hoon ; Kwangwoon University, School of Robotics Sohn, Daewon; Hanyang University, Department of Chemistry Laurell, Thomas; Lund University, Biomedical Engineering; The University of Tokyo; Universiti Putra Malaysia Ota, Sadao; The University of Tokyo, Research Center for Advanced Science and Technology Lee, sangwook; Inje University - Gimhae Campus, Bio-health Product Research Center; The University of Tokyo, RCAST

Reduced acoustic resonator dimensions improve focusing efficiency of bacteria and submicron particles

Masashi Ugawa[a], Hoyeon Lee[b] ,Thierry Baasch[c] ,Minho Lee[d], Soyun Kim[e,f], OkChan Jeong[g], Yong-Hoon Choi[h], Daewon Sohn[b], Thomas Laurell[c], Sadao Ota*[a], SangWook Lee*[a,i]

[a] RCAST, The University of Tokyo, 153-8904, Tokyo, Japan

[b] Department of Chemistry, Research Institute for Convergence of Basic Science, Hanyang University, Seoul, 04763, Korea

[c] Department of Biomedical engineering, Lund University, 22363, Lund, Sweden

[d] School of integrative engineering, Chung-Ang University, Seoul, 06974, Korea

[e] Convergence Research Institute, Korea University, 02841,Seoul, Korea

[f] *PCL Inc*., 05854, Seoul, Korea

[g] Department of Biomedical Engineering, Inje University, Gimhae-si, 50834, Korea

[h] School of Robotics, KwangWoon University, 01897, Korea

[i] Bio-health Product Research Center, Inje University, Gimhae-si, 50834, Korea

Corresponding: sadaota@solab.rcast.u-tokyo.ac.jp & swlee@g.ecc.u-tokyo.ac.jp

In this study, we demonstrate an acoustofluidic device that enables single-file focusing of submicron particles and bacteria using a two-dimensional (2D) acoustic standing wave. The device consists of a 100 μm × 100 μm square channel that supports 2D particle focusing in the channel center at an actuation frequency of 7.39 MHz. This higher actuation frequency compared with conventional bulk acoustic systems enables radiation-force-dominant motion of submicron particles and overcome the classical size limitation (≈ 2 μm) of acoustic focusing. We present acoustic radiation force-based focusing of particles with diameters less than 0.5 μm at a flow rate of 12 μL min^{-1}, and 1.33 μm particles at flow rates up to 80 μL min^{-1}. The device focused 0.25 μm particles by the 2D acoustic radiation force while undergoing a channel cross-section centered, single-vortex acoustic streaming. A suspension of bacteria was also investigated to evaluate the biological relevance of the device, which demonstrated the alignment of bacteria in the channel at a flow rate of up to 20 μL min^{-1}. The developed acoustofluidic device can align submicron particles within a narrow flow stream in a highly robust manner, validating its use as a flow-through focusing chamber to perform high-throughput and accurate flow cytometry of submicron objects.

Keyword: Square microchannel, Acoustophoresis, submicron particles, Flow cytometry, Acoustic radiation, Acoustic streaming

Introduction

Flow cytometry enables the analysis of large numbers of cells within a fluid stream[1,2]. Recently, this technique has been used in various applications to measure a diverse range of chemical and physical characteristics of individual cells[3], including the diagnosis of blood cancer, cell phenotyping, cell cycling, and rare cell detection[4]. Flow cytometry involves the use of a device for accurately focusing a cell stream and an optical setup for single-cell level detection[2], enabling the measurement of single cells or micron-sized particles as they pass through an optical detection volume. Thus, it is critically important to focus the sample (cells or particles) in a narrow core stream of cells, precisely positioned in the interrogation zone, to improve the measurement resolution of the cells [5].

A single-file coaxial hydrodynamic flow chamber is a widely used focusing method in conventional flow cytometry [6,7]. Many attempts have been made to replace this conventional flow chamber with microfluidic devices [8,9] with various microfluidics-based focusing approaches such as 3-D hydrodynamic [10,11], inertial[12,13], non-Newtonian[14-17] magnetic[18,19], dielectrophoretic[20,21], and acoustic[22,23]. Among them, the acoustics-based approach has advantages in terms of high throughput, simplicity, precise manipulation, and gentle treatment of cells[23]. The combination of acoustic radiation forces acting on suspended objects streaming in microchannels (Fig. 1) is commonly referred to as acoustofluidics. The acoustic radiation force can manipulate particles according to their size, density, and compressibility differences between the particles and the suspending medium[24]. Because of capabilities such as alignment[25], trapping[26], and orientation of particles in the microchannel, acoustofluidics has numerous biological applications such as plasmapheresis[27,28], lipid separation[29], isolation of circulating tumor cells[30,31], bacterial separation[32,33], and orientation of red blood cells[34,35]. Moreover, acoustofluidics operates independently of the biochemical and electrical properties of the suspending medium and has been extensively explored in various biological samples, including blood, urine, cerebrospinal fluid, raw milk, and water resources[36-38]. However, manipulations or focusing of cells in the submicron range using acoustofluidic methods are limited because, as the particle size decreases, the physical scaling laws that govern the acoustic radiation force decay faster than the hydrodynamic viscous drag force induced by acoustic streaming, thereby counteracting the focusing properties of the radiation force.

In general, the motions of larger particles (>2 μm) are dominated by the acoustic radiation force, while those of smaller particles are dominated by the drag force induced by acoustic streaming in the suspending media[39]. Therefore, focusing of submicron range bio-objects such as bacteria, viruses, and even exosomes is impaired by the interplay between the acoustic radiation force and the viscous drag force from acoustic streaming. Several systems have been developed to overcome this limitation, including acoustic seed trapping[40], diffraction-based acoustic manipulation[41], and combining acoustic radiation and an acoustic streaming vortex[42,43]. Antfolk *et al.*[42] demonstrated a square cross-section (230 × 230 μm) silicon-glass microchannel operated by a bulk acoustic wave (BAW) that focused submicron particles and bacteria. The chip was able to focus 0.5 μm particles toward the channel center because of the fact that conventional Rayleigh streaming, arising in a half-wavelength acoustic

resonator, reconfigured to a cross-section centered single-vortex stream when operated in a two-dimensional acoustic resonator setup; hence, it does not interfere with the acoustic radiation force directed toward the channel center. The maximum flow rate allowing focusing of 0.5 µm particles was less than 2 µL min^{-1} (~3.3 mm s^{-1}). The focusing efficiency in this configuration depends on the magnitude of the radiation force and the retention time in the force field. Similarly, Zangming et al.[43] developed an acoustofluidic chip for the enrichment of submicron particles using a square-shaped capillary tube on a chirped surface acoustic wave (SAW) transducer. The SAW induced a torsional vibration mode in the square glass capillary that generated a single-vortex acoustic streaming in the capillary. The enrichment of submicron to nanoparticles was demonstrated under stop-flow or extremely low-flow conditions and were not readily applicable to high-speed flow cytometry.

The simplest approach to overcome the particle size limitation problem in a one-dimensional (1D) BAW resonance is to reduce the boundary driven Rayleigh streaming. The relationships between the acoustic radiation force and streaming-induced drag force on particle motion in 1D acoustophoresis systems have been studied in detail theoretically[39] and experimentally[44-46]. The authors presented the critical particle diameter $2a_c$ to define the shift from radiation force-dominated particle motion to acoustic streaming-induced particle motion. Equation 1 shows the critical diameter derived when the magnitudes of the two forces are equal at the center plane in a 1D half-wavelength resonance:

$$2a_c = \sqrt{\frac{12sv}{\pi\phi f}} \quad (1)$$

where s is a factor related to the channel geometry, v is the kinematic viscosity of the media, Φ is the acoustic contrast factor, and f is the frequency of the acoustic field. The equation shows that the critical particle size can be decreased by operating at a higher frequency (f), changing the properties of the medium (v, Φ)[47], or adjusting the channel geometry (s)[48]. A graphical illustration of this relationship is presented in Fig. 1.

To circumvent the size limitations for acoustic focusing, in the classical 1D resonance-driven Rayleigh streaming, we developed an acoustofluidic device in which the microchannel size was reduced to 100 µm × 100 µm compared with previous work[42], to obtain a $\lambda/2$ resonance with a pressure node at the channel center. The system was operated at 7.39 MHz. Based on equation (1), the critical particle size ($2a_c$) can be calculated as approximately 1.0 µm for a polystyrene particle in water at a frequency of 7.39 MHz (f) and geometric factor of 0.47 (s) used for a square cross-section as in the ref 42. In the context of a square cross-section channel, we expected to obtain a unidirectional vortex streaming in the channel cross-section that would not counteract the acoustic radiation force-driven particle trajectory toward the channel center. Hence, a higher speed of focusing submicron particles was expected compared with previous reports[42], allowing operation at an increased flow rate. Using the device, we investigated and demonstrated focusing of microsized beads (3.25 µm and 1.33 µm in diameter) and further submicron sized beads (0.5 µm, 0.25 µm, and 0.191 µm) under different flow

conditions (flow rate from 10 µL min^{-1} (linear flow rate: 17 mm s^{-1} to 80 µL min^{-1} (linear flow rate: 133 mm s^{-1})). We observed and analyzed the particle location in flow-through mode to investigate the focusing efficiency of the device. Finally, we examined the focusing features of bacteria to explore the biological relevance of the device.

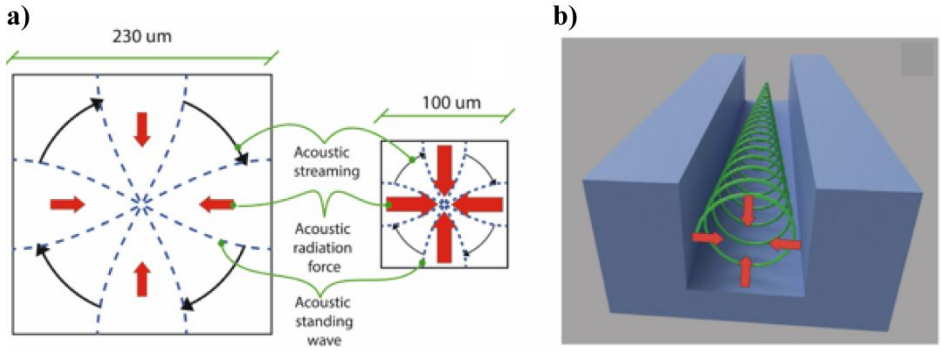

Fig. 1 a) 2D acoustic resonance (dashed blue lines) in a channel with a square cross-section. Black arrows indicate unidirectional acoustic streaming. Red arrows indicate the direction of the acoustic radiation force. The smaller cross-section yields a higher resonance frequency and hence a higher radiation force, even though still complemented by an axicentric acoustic streaming roll. b) Schematic of the spiral-shaped trajectory of nanoparticles (green) that converges toward the channel centerline under the influence of the acoustic radiation force.

Experimental

Acoustofluidic chip

Figure 2(a) shows the acoustofluidic device consisting of a main fluidic channel and two fluid ports, which was fabricated by bonding a glass-silicon-glass sandwich structure. First, silicon wafers with a thickness of 100 µm were prepared using a chemical-mechanical polishing process for a double-side-polished 4 inch silicon wafer with a thickness of 400 µm. A silicon microchannel structure with a cross-section of 100 µm × 100 µm was subsequently fabricated by deep reactive ion etching through a silicon wafer. The fabricated microchannel structure was sequentially sealed by anodic bonding of a bottom layer of borosilicate glass (10 mm × 80 mm × 0.5 mm). The top layer of borosilicate glass was provided with through-holes as the inlet and outlet ports and was bonded on the structure by anodic bonding. A 5 mm × 10 mm piezoelectric transducer (C-213; Fuji Ceramics) was glued to the bottom glass layer along the microfluidic channel using cyanoacrylate glue (AD100; 3M).

Acoustophoresis setup

Figure 2(b) shows the experimental setup. The electrical signal for piezoelectric actuation was generated by a single-channel functional generator (WF 1974, NF Corporation, Japan) set to 7.39 MHz,

and further amplified using a power amplifier (BA 4850, NF Corporation, Japan). The amplified signal was set to 50 $V_{p\text{-}p}$, which is the maximum amplitude to prevent the chip heating induced by thermal losses in the piezoceramic element. Because the piezoelectric actuator simultaneously excited a vertical and horizontal resonance in the chip owing to the square cross-section of the channel, cells or particles were focused at the center of the microfluidic channel.

The flow rates of the working fluid containing beads and bacteria samples were controlled by syringe pumps (70-4505 Elite Pump; Harvard Apparatus) mounted with syringes (SS05-LZ; Terumo) connected to the inlets and outlets of the microfluidic channel. The inlets and outlets were directly connected to the syringes by polyetheretherketone tubes. To prevent unwanted bubble entrapment, the channels were filled with deionized water prior to experiment. After device preparation, syringes containing the samples were loaded. Various flow rates of the working fluid were supplied to the device from 5 µL min^{-1} to 80 µL min^{-1}. Video images of flowing cells were obtained at 5 cm from the inlet port (observation area in Fig. 2(b)) in the channel using a CMOS camera (Miro lab 110 of Vision Research, USA) linked to the microscope (Olympus BX51, Japan).

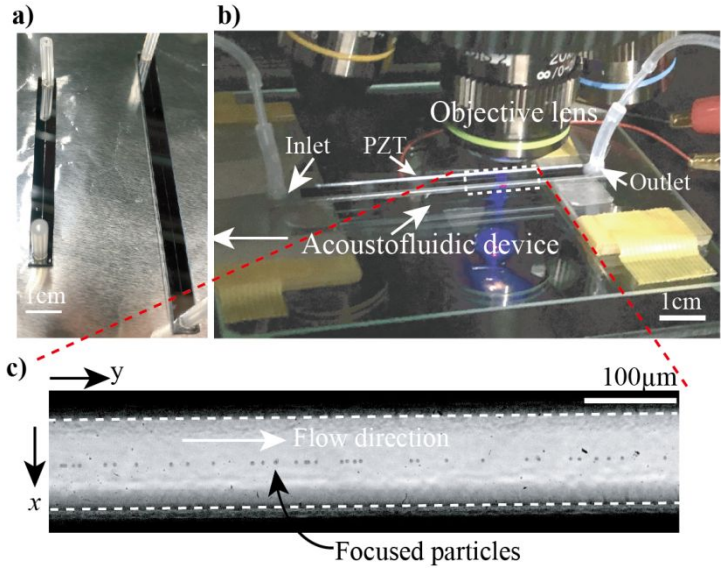

Fig. 2 a) Acoustofluidic devices with length of 50 mm or 75 mm, width of 5 mm, thickness of 1.1 mm, and square-shaped microchannel cross-sections (100 µm ×100 µm). b) Experimental setup: A syringe pump is linked to the inlet port for sample introduction, and a waste tube is linked to outlet. A CMOS camera mounted to a microscope recorded the acoustofluidic channel. c) Top view of a sample with 3.25 µm polystyrene beads, perfused at 30 µL min^{-1}, focused inside the channel while operating the PZT at 7.395 MHz.

Microbeads

Polystyrene microparticles of various sizes were used to characterize the system. Particles with diameters of 3.25 µm, 1.33 µm, and 0.25 µm were obtained from Spherotech (FP-3052-2, FP-1552-2, and FP-256-2, respectively; Spherotech Inc., IL, USA). Particles with diameters of 0.5 µm and 0.191 µm were obtained from Bang Laboratories (FSDG002 and FSDG003, respectively; Bang Laboratories,

Fishers, IN, USA). Particle concentrations were kept below 10^9 particles mL^{-1} to minimize the effect of acoustic and hydrodynamic interaction forces between particles.

Bacteria

Bacteria were purchased from the Korean Collection for Type Cultures (KCTC). *Enterobacter cloacae* was grown at 30 °C in nutrient broth medium. The bacteria were cultured under aerobic conditions up to an optical density of 0.4 at 600 nm (OD_{600}), followed by centrifugation (~14,200 g) for 10 min at 4 °C, and then washed twice with Tris-HCl buffer (50 mM Tris, pH 7.4, 1 mM $MgCl_2$, 5 mM KCl, 100 mM NaCl).

Result and Discussion

Acoustophoresis

Acoustophoresis refers to the movement of suspended particles in a fluid through acoustic radiation forces. This enables the enrichment of particles, particle transfer from one carrier fluid to another, or particle isolation according to their size, density, or compressibility[49]. Acoustic radiation forces are produced by a piezoelectric actuator that vibrates the microfluidic device at the resonance frequency of the fluid-filled channel. The particles in suspension experience a force along the direction of the pressure gradient generated by the acoustic standing wave, transferring them to either the pressure minima or maxima depending on their acoustic properties. We set up a model of the channel cross-section in finite-element software COMSOL Multiphysics 5.5 to investigate the interplay between acoustic radiation forces and streaming. We followed the approach by Baasch et al.[50] to model the acoustic streaming while dropping the thermal effects and the approach by Antfolk et al.[42] regarding the model of the channel cross section and the respective boundary conditions.

The setup (Fig. 3a) consists of the quadratic channel cross-section. As a boundary condition, we applied a velocity in the wall normal direction, opposite walls are moving in phase and while we set a $\pi/2$ phase difference between vertical and horizontal walls. The velocity amplitude was chosen to be 0.001 m/s which leads to a pressure amplitude of 0.6 MPa at the resonance frequency of 7.45 MHz. A rotating pressure field is generated (Fig. 3b) when the horizontal and vertical walls move out of phase, as was shown by Antfolk et al[42]. This rotating pressure field generates a Gorkov potential with a local minimum at the center of the capillary cross section (Fig. 3c) and a rotating streaming field (Fig. 3d). The Gorkov potential as shown in Fig. 3c was computed for 100 µm radius polystyrene particles. When balancing the average acoustic radiation force (outside the viscous boundary layer close to the channel walls) with the average acoustic streaming force (by using the Stokes drag) we found a critical radius between 0.31 µm and 0.32 µm for polystyrene particles in this 100 µm by 100 µm cross section. In an analogous model of a 400 µm by 400 µm channel cross-section we found the critical radius to be between 0.625 µm and 0.645 µm.

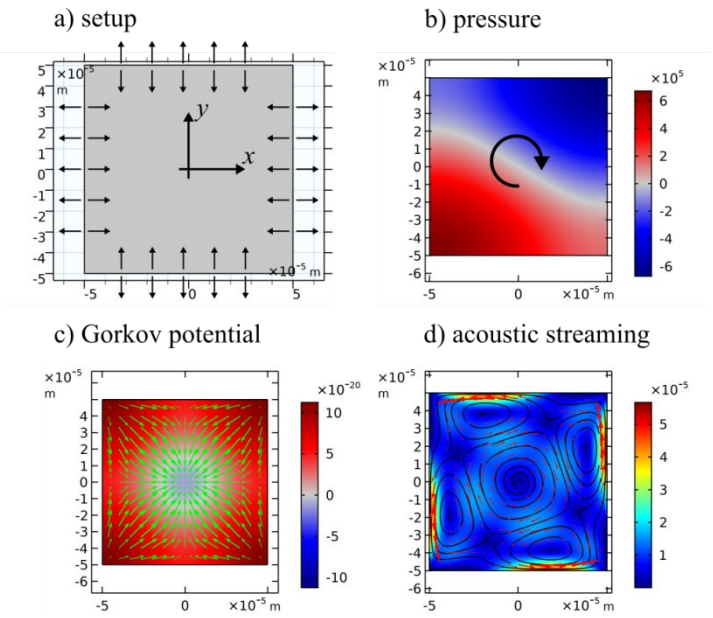

Fig. 3 a) In our numerical model we only considered the quadratic channel cross section. b) The phase difference between vertical and horizontal wall excitation generates a rotating pressure field. c) The rotating pressure field in turn generates a Gorkov potential with a local minimum at the center of the channel. d) The (Eulerian) acoustic streaming is shown in panel.

2D acoustic focusing

The single transducer can excite both vertical and horizontal $\lambda/2$ standing waves because the microchannel has a square cross-section (100 µm × 100 µm). Fig 2 shows two acoustofluidic devices (Fig 2-a), the experimental setup (Fig 2-b), and focused particles (Fig 2-c) during the experiment. The 2D resonance mode drives the particles to the pressure node at the channel center, as shown in Fig. 2-c, and achieves a continuous-flow-based deviation-free center location of particles in the optical focal plane, which is crucial for flow cytometry applications.

To investigate the focusing performance of the microchannel, particles with diameters of 3.25 µm, 1.33 µm, 0.5 µm, 0.250 µm, and 0.191 µm were each perfused through the device. The flow rate ranged from 10 µL min^{-1} to 80 µL min^{-1}, while the peak-to-peak voltage applied to the transducer remained constant. The flowing particles were observed using an objective lens with a high numerical aperture (20x, N.A. 0.75) connected to the high-speed camera at the top. We first conducted focusing tests of the device using particles larger than 1 µm, i.e., 3 µm and 1.33 µm in diameter.

Figure 4 presents images of the particles focused toward the channel center. The images were obtained using a high-speed camera set to a frame rate and exposure time of 1000 fps and 20 µs, respectively. The lateral distribution of each particle was measured from the images (Supplementary Information, Figure S-1). Particle analysis was performed on the obtained videos using Trackpy (v0.4.2)[51]. First, the particles in all frames were detected, and the particles detected in each frame were linked to those detected in consecutive frames. Then, the intersection of each particle at a designated cross-sectional position of the channel was obtained by interpolating the particle trajectory. Based on the histogram, we calculated the standard deviation of the particle distribution (σ) and defined 2σ as

the focusing width, Fig 4-b.

For all investigated flow rates, the 3.25 µm particles were tightly focused within 2 µm at the center of the fluid channel. The focusing width of the 1.33 µm particles increased with the increase in flow rate. The focusing width was 10 µm at a flow rate of 80 µL min^{-1}, corresponding to a linear average velocity of 13.3 cm s^{-1}. The acoustofluidic device showed excellent 2D focusing even for the 1.33 µm particles.

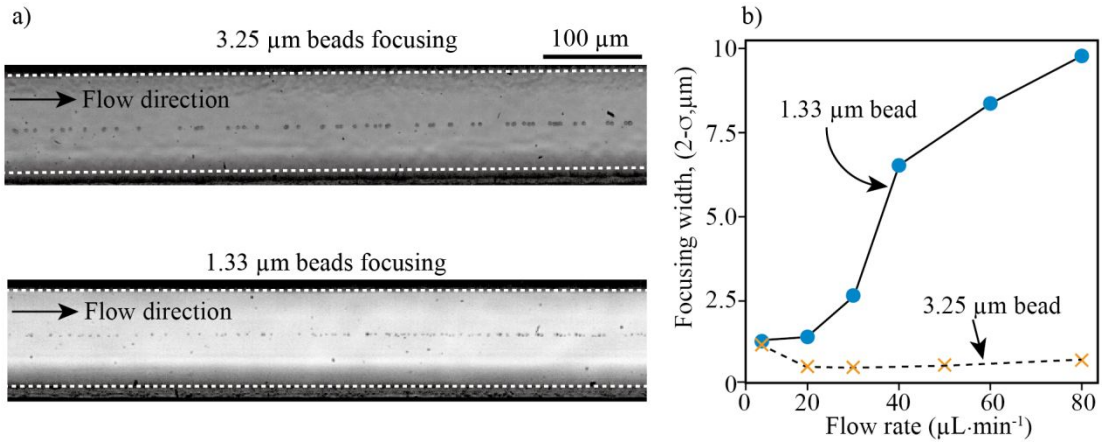

Fig. 4 a) Focusing images of 3.25 µm and 1.33 µm particles, showing tight focusing even at a flow rate of 80 µL min^{-1}. b) Focusing width of each particle size at flow rates ranging from 10 µL min^{-1} to 80 µL min^{-1}. Focusing width is defined as the standard deviation of the lateral particle distribution. At a flow rate of 80 µL min^{-1}, the 3 µm particles deviated by less than 1 µm from the centerline, while the 1.33 µm particles displayed a 10 µm focusing width. (2σ standard deviation)

Figure 5 shows the focusing sequence of 0.5 µm particles at stop-flow before and after the acoustic actuation. To investigate the movement of particles with diameters less than 0.5 µm, fluorescence microscopy was employed to visualize the movement. The movements of three different submicron particles (0.5 µm, 0.25 µm, and 0.191 µm) were observed under stop-flow conditions, while acoustic actuation was applied to the chip. Visually, it can be observed that the 0.5 µm particle moved rapidly toward the centerline and was moderately influenced by the rotating streaming vortex owing to the short transition time to the channel center. In contrast, the smaller particles showed a gradual focusing toward the centerline while simultaneously following the acoustic streaming-induced fluid rotation (see supplementary video: Video.1 for 0.25 µm and Video.2 for 0.191 µm).

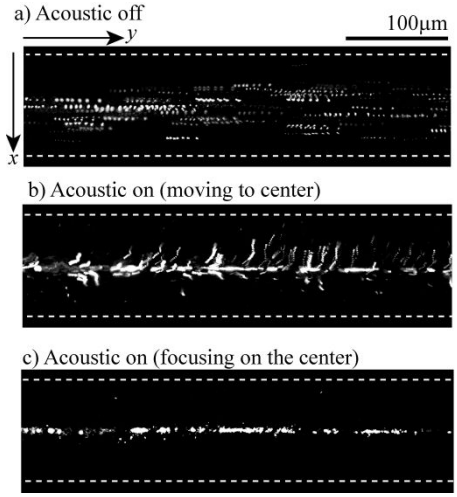

Fig. 5 Time-lapse images of 0.5 μm particle movement under both acoustic-off and acoustic-on conditions by an acoustic actuation a) Particles were distributed randomly and moved by a pressure driven flow in the channel without any acoustic actuation active. b) Tracing images show that the particles moved toward the channel center by applying an RF frequency to generate an acoustic standing wave. c) In the end, the particles were focused and enriched at the channel center.

Figure 6 illustrates the results of the focusing performance of 0.5 μm particles at different flow rates. The particles could be fully focused in a single streamline at the channel center at a flow rate of 8 μL min^{-1}; however, at 12 μL min^{-1}, the retention time in the acoustic field was insufficient to fully focus all particles. The corresponding linear velocities (average velocities) at 8 μL min^{-1} and 12 μL min^{-1} were 1.33 cm s^{-1} and 2 cm s^{-1}, respectively. The focusing efficiency can be further improved if an active cooling system is installed, which enables the operation of the piezoelectric actuator at a higher driving voltage without the thermal dissipation, which may lead a resonance shift[52].

In addition, while we observed that 0.25 μm and 0.191 μm particles can be focused toward the centerline of the square cross-section channel under stop-flow, the maximum flow rate while still having sufficient focusing depends on the retention time in the acoustic field. The time it takes to reach the centerline of the microchannel is inversed-proportional to the acoustic velocity, and hence the square of the particle radius (Eq. 4). In the experiment, both the 0.25 μm and 0.191 μm particles were injected into the device, and focusing tests were conducted in the flow-through mode. The 0.25 μm particles were focused at a flow rate of 2 μL min^{-1}, which is in agreement with the reduced acoustophoretic velocity compared with that of the 0.5 μm particles. A factor of two reduced radii should yield a factor of four lower acoustophoretic velocity, which provides the corresponding extended retention time in the acoustic field. Under the given actuation and fluidic conditions, the focusing of 0.191 μm particles was too slow to be observed in the flow-through mode.

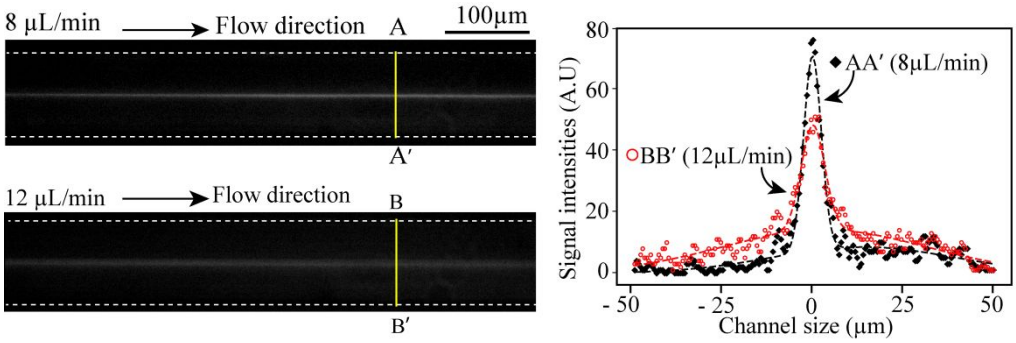

Fig. 6 a) Images of focusing of 0.5 μm particles under two different flow conditions (8 μL min^{-1} and 12 μL min^{-1}). b) . AA' and BB' are cross section of each channel and cross-sectional profiles of fluorescent intensity displayed at these flow conditions

Bacteria focusing

Figure 7(a) shows images of acoustic focusing bacterial cells at different flow rates. A suspension of *Enterobacter cloacae* was investigated to evaluate the biological relevance of the device. Bacteria samples were vortexed prior to injection to prevent aggregation. The sample concentration was 10^8 cells mL^{-1}, which is sufficient to visualize the stream of bacterial flows by bright field observation (without fluorescent dye).

Figure 7(b) illustrates focusing width of the bacterial cells as a function of the flow rate, which was obtaining by analyzing the focused bacterial streams in the images. An analysis to obtain the flow position of bacteria was performed as follows. First, the intensity profile at the designated cross-section of the channel was obtained. After subtracting the background, peak detection was performed on the profile to determine the cross-section of the bacteria at a certain frame. Finally, the positions of the peaks in each frame were combined to obtain the histogram (S-2). The standard deviations of each histogram were calculated based on the histogram and 2-σ of each image was plotted as their focusing width. While the features of performing bacteria focusing were analyzed by observing its focused streamline due to a limited optical setup used in this study, our acoustofluidic device enables observation of bacteria at single cell resolutions by installing high magnification and high N.A. objective lenses.

As a result, the focusing width was approximately 3.6 μm at a flow rate of 5 μL min^{-1}, and reached 6 μm at 20 μL min^{-1}. The calculated flow averaged velocity at 20 μL min^{-1} was 3.33 cm s^{-1}, demonstrating that the developed device can operate as a high-speed and high-throughput focuser of submicron cells. In contrast to commercial flow cytometry, in which flow focusing relies on the use of large volumes of hydrodynamic sheath flow, acoustofluidics enables the focusing of bacteria and submicron particles without requiring such sheath flow.

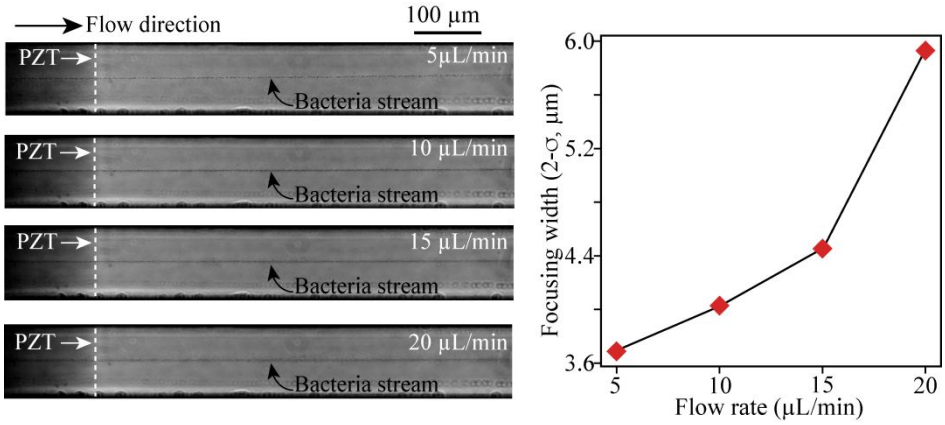

Fig. 7 a) Image of bacteria flow stream obtained at four different flow conditions. b) The focusing width, 2-σ of bacterial distribution, plotted at four different flow rates. At a 5 μL min^{-1} flow rate, the measured focusing width 2-σ was about 3.6 μm, and reached 6 μm at a 20 μL min^{-1}.

Conclusions

This paper presents an acoustofluidic device with a square channel structure (100 μm × 100 μm) that achieves 2D acoustic focusing of submicron particles by using a single piezoelectric actuator. At a 7.39 MHz actuating frequency, 0.5 μm polystyrene particles were rapidly focused toward the channel center by the acoustic radiation force. 0.25 μm particles underwent an extensive vortex rotation driven by acoustic streaming due to the longer elapsed time for the particle to get to the channel center by acoustic focusing.

The current device can focus particles with diameters down to 0.5 μm nm for a fast retention time in a 75 mm focusing channel at a linear flow rate of 13 mm s^{-1} and 0.25 μm particles at a linear flow rate of 2 μL min^{-1}. This enables to open up the acoustophoresis research field to new application in microbiology such as microalgae, plankton, and bacteria. Future work will target an improved optical system to develop a single-cell resolution flow cytometry system for submicron cells and particles.

Author contribution

M. Ugawa conducted experiment and analysis of data. H. Lee did experiment and data acquisition. T. Baasch conducted modelling and simulation. M. Lee & S.Kim proposed the idea and experimental step. O.K. Jeong conducted and advised fluidic experiment. Y.H. Cho did image analysis of the experiments. D.W. Sohn proposed and advised the experimental methods. T. Laurell wrote paper and advised all experiment. S. Ota & S.W Lee proposed the idea, wrote the paper and managed whole process.

Acknowledgements

This work was supported by the Korean Ministry of Environment (Grant no. RQ201901136). This work was also supported by JST, CREST Grant Number JPMJCR19H1, Japan.

Conflicts of interest

There are no conflicts to declare

References

1. A. Adan, G. Alizada, Y. Kiaz, Y. Baran, A. Nalbant, Flow cytometry: basic principles and applications, Cri Rev Biotechnol, 2017 **37** 163-176

2. N. Barteneva, E. Fasler-Ken, I.A. Vorojev, Imaging flow cytometry: copying with heterogeneity in biological systems, Journal of Histochemistry & Cytochemistry 2012 **60** 723-733

3. S. S. Khan, M. A. Solomon, J. P. McCoy, Jr, Detection of circulating endothelial cells and endothelial progenitor cells by flow cytometry, Cytometry Part B 2005 **64** B1-8

4. C. D Jennings, K.A. Foon, Recent Advances in Flow Cytometry: Application to the Diagnosis of Hematologic Malignancy, Blood 1997 **90** 2863-2892

5. Y. Gong, N. Fan, X. Yang, B. Peng, H. Jiang, New advances in microfluidic flow cytometry, Electrophoresis 2018 **22** 1212-1229

6. H.K. Kruth, Flow cytometry: Rapid biochemical analysis of single cells, Analytical Biochemistry 1982 **125** 225-242

7. J.A. Steinkamp, Flow cytometry, Review of Scientific Instruments 1984 **55** 1375

8. S. Stravrakis, G. Holzner, J. Choo, A. deMello, High-throughut microfluidic imaging flow cytometry, Current Opinion in Biotechnology 2019 **55** 36-43

9 X. Xuan, J. Zhu, C. Church, Particle focusing in microfluidic device, Microfluidics and Nanofluidics 2010 **9** 1-16

10. Y.J. Chiu, S.H. Cho, Z. Mei, V. Lien, T.F. Wu, Y.H. Lo, Universally applicable three-dimensional hydrodynamic microfluidic flow focusing, Lab Chip, 2013 **13** 1803-1809

11. M.A. Daniel, D.A. Boyd, D.R. Mott, F.S. Ligler, 3D hydrodynamic focusing microfluidics for emerging sensing technologies, Biosensors and Bioelectronics 2015 **67** 25-34

12. D.D. Carlo, Inertial microfluidics, Lab. Chip. 2009 **9** 3038-3046,

13. J. Zhang, S. Yan, D. Yuan, G. Alici, N.T. Nguyen, M.E. Wakiani, W. Li, Fundamentals and applications of inertial microfluidics: a review, Lab. Chip. 2016 **16** 10-34

14. G. Holzner, S. Stavrakis, A. deMello, Elesto-Inertial focusing of mammalian cells and bacteria using low molecular, low viscosity PEO solutions, Anal. Chem. 2017 **89** 11653-11663

15. S. Yang, J.Y. Kim, S.J. Lee, S.S. Lee, J.M. Kim, Sheathless elasto-inertial particle focusing and continuous separation in a straight rectangular microchannel, Lab. Chip. 2011 **11** 266-273

16. D. Yuan, Q. Zhao, S. Yan, S.Y. Tang, G. Alici, J. Zhang, W. Li, Recent progress of particle migration in viscoelastic fluids, Lab. Chip. 2018 **18** 551-567

17. N. Xiang, X. Zhang, Q. Dai, K. Chen, Z. Ni, Fundamentals of elasto-inertial particle focusing in curved microfluidic channels, Lab. Chip. 2016 **16** 2626-2635

18. L. Luo, Y. He, Magnetically Induced Flow Focusing of Non-Magnetic Microparticles in Ferrofluids under Inclined Magnetic Fields, Micromachines 2019 **10** 56

19. A. Rodríguez-Villarreal, M. Tarn, L.A. Madden, J. Lutz, J. Greenman, J. Samitier, N. Pamme, Flow focusing of particles and cells based on their intrinsic properties using a simple diamagnetic repulsion setup, Lab. Chip. 2011 **11** 1240-1248

20. S. Yan, J. Zhang, M. Li, G. Alici, H. Du, R. Sluyter, W. Li, On-chip high-throughput manipulation of particles in a dielectrophoresis-active hydrophoretic focuser, Scientific Report 2014 **4** 5060

21. J. Zhu, X. Xuan, Dielectrophoretic focusing of particles in a microchannel constriction using DC-biased AC electric field, Electrophoresis 2009 **30** 2668-2675

22. M. Wu, A. Ozcelik, J. Rufo, Z. Wang, R. Fang, T.J. Huang, Acoustofluidic separation of cells and particles, Microsystems & Nanoengineering 2019 **5** 32

23. A. Lenshof, C. Magnusson, T. Laurell, Acoustofluidics 8:Applications of acoustophoresis in continuous flow microsystems, Lab. Chip. 2012 **12** 1210-1223

24. H. Bruus, Acoustofluidics 1: Governing equations in microfluidics, Lab Chip 2011 **11** 3742-3751

25. C. Grenvall, C. Antfolk, C. Z. Bisgaard, Thomas Laurell, Two-dimensional acoustic particle focusing enables sheathless chip Coulter counter with planar electrode configuration, Lab Chip, 2014 **14** 4629-4637

26. D. Bazou, L.A. Kuznetsova, W.T. Coakley, Physical enviroment of 2-D animal cell aggregates formed in a short pathlength ultrasound standing wave trap, Ultrasound Med. Biol. 2005 **31** 423-430

27. J. Nam, H. Lim, D. Kim, S. Shin, Separation of platelets from whole blood using standing surface acoustic waves in a microchannel, *Lab Chip* 2011 **11** 3361-3364

28. A. Lenshof, A. Ahmad-Tajudin, K. Jaras, A.M. Nilsson, L. Aberg, G. Marko-Varga, J. Malm, H. Lilia, T. Laurell, Acoustic Whole Blood Plasmapheresis Chip for Prostate Specific Antigen Microarray Diagnostics, Anal. Chem. 2009 **81** 6030-6037

29. F. Petersson, A. Nilsson, C. Holm, H. Jonsson, T. Laurell, Continuous separation of lipid particles from erythrocytes by means of laminar flow and acoustic standing wave forces, *Lab Chip* 2005 **5** 20-22

30. M. Antfolk, C. Magnusson, P. Augustsson, H. Lilja, T. Laurell, Acoustofluidic, Label-Free Separation and Simultaneous Concentration of Rare Tumor Cells from White Blood Cells, Anal. Chem. 2015 **87** 9322-9328

31. M. Wu, P.H. Huang, R. Zhang, Z. Mao, C. Chen, G. Kemeny, P. Li, A.L. Lee, R. Gyanchandani, A.J. Armstrong, M. Dao, S. Suresh, T. Huang, Circulating Tumor Cell Phenotyping via High-Throughput Acoustic Separation, Small 2020 **27** 2004438

32. S. Li, F. Ma, H. Bachman, C.E. Cameron, X. Zeng, T. Huang , Acoustofluidic bacteria separation, J. Micromech. Microeng. 2017 **27** 015031

33. P. Ohlsson, K. Petersson, P. Augustsson, T. Laurell, Acoustic impedance matched buffers enable separation of bacteria from blood cells at high cell concentrations, Scientific Report 2018 **8** 9156

34. L.G. Rico, J. Junca, M.D. Ward, J.A. Bradford, J. Bardina, J. Petriz, Acoustophoretic Orientation of Red Blood Cells for Diagnosis of Red Cell Health and Pathology, Scientific Research 2018 **8** 15705

35. O. Jakobsson, M. Antfolk, T. Laurell, Continuous Flow Two-Dimensional Acoustic Orientation of Nonspherical Cells, Anal. Chem. 86 (2012) 6111-6114

36. C. Grenvall, J.R. Folkenberg, P. Augustsson, T. Laurell, Label-free somatic cell cytometry in raw milk using acoustofluidics, Cytometry A 2012 **81** 1076-1083

37. Z. Wang, J. Rufo, C. Chen, S. Yang, S. Yang, L. Li, J. Zhang, J. Cheng, Y. Kim, M. Wu, E. Abemayor, M. Tu, D. Chia, R. Spruce, N. Batis, H. Mehanna, D. Wong, T. Huang, Acoustofluidic salivary exosome isolation, The journal of molecular diagnosis 2020 **22** 50-59

38. J.W. Park, S.H. Kim, T. Ito, T. Fujii, S.H. Kim, S.W. Lee, K. Goda, Acoustofluidic harvesting of microalgae on a single chip, Biomicrofluidics 2016 **10** 034119

39. P.B. Muller, R. Barnkob, M.J.H. Jensen, H. Bruus, A numerical study of microparticle acoustophoresis driven by acoustic radiation forces and streaming-induced drag forces, Lab. Chip 2012 **12** 4617–4627

40. B. Hammastrom, T. Laurell, J. Nilsson, Seed particles-enabled acoustic trapping of bacteria and nanoparticles in continuous flow system, Lab Chip 2012 **12** 4296-4304

41. C. Devendran, K. Choi, J. Han, Y. Ai, A. Neild, D.J. Collins, Diffraction-based acoustic manipulation in microchannels enables continuous particle and bacteria focusing, Lab Chip 2020 **20** 2674-2688

42. M. Antfolk, P.B. Muller, P. Augustsson, H. Bruus, T. Laurell, Focusing of sub-micrometer particles and bacteria enabled by two-dimensional acoutophoresis, Lab Chip 2014 **14** 2791

43. Z. Mao, P. Li, M. Wu H. Bachman, N. Mesyngier, X. Guo, S. Liu, F. Costanzo, T. Huang, Enrichment nanoparticles via acoustofluidics, ACS Nano 2017 **11** 603-612

44. R. Barnkob, P. Augustsson, T. Laurell, H. Bruus, (2012) Acoustic radiation and streaming induced microparticle velocities determined by microparticle image velocimetry in an ultrasound symmetry plane, Phys. Rev. E, 2012 **86** 056307

45. P.B. Muller, M. Rossi, A.G. Marin, R. Barnkob, P. Augustsson, T. Laurell, C.J. Kahler, H. Bruus, Ultrasound-induced acoustophoretic motion of microparticles in three dimensions. Phys. Rev. E 2013 **88** 023006

46. M.Settens and H.Bruus, Forces acting on a small particle in an acoustical field in a viscous fluid ,Phys. Rev. E 2012 **85** 016327

47. D. van Assche, E. Reithuber, W. Qui,T. Laurell, B. Henriques-Normark B, Mellroth, P. Ohlsson, P. Augustsson, Gradient acoustic focusing of sub-micron particles for separation of bacteria from blood lysate, Scientific Report 2020 **10** 3670

48. P.B. Muller, R. Barnkob, M.J.H Jensen, H. Bruus, A numerical study of microparticle acoustophoresis driven by acoustic radiation forces and streaming-induced drag forces, Lab Chip 2012 **12** 4617

49. A. Urbansky, P.Ohlsson, A. Lenshof, F. Garofalo, S. Scheding, T. Laurell, Rapid and effective enrichment of mononuclear cells from blood using acoustophoresis, Scientific Reports 2017 **7** 17161.

50. T. Baasch, A. Pavlic, J. Dual, Acoustic radiation force acting on a heavy particle in a standing wave can be dominated by the acoustic microstreaming, Physical Review E 2019 **100.6** 061102.

51. D. Allan et al., soft-matter/trackpy:Trackpy v0.4.2, Zendo 2019, http://doi.org/10.5281/zenodo.3492186

52. P.Augustsson, C. Magnusson, M Nordin, H. Lilja, T. Laurell, Microfluidic, label-free enrichment of prostate cancer cells in blood based on acoustophoresis, Anal. Chem. 2012 *84* 7954-7962